A Comparison between Polarimetric Radar and Wind Profiler Observations of Precipitation in Tropical Showers

PETER T. MAY

Bureau of Meteorology Research Centre, Melbourne, Victoria, Australia

A. R. JAMESON

RJH Scientific, Inc., Alexandria, Virginia

THOMAS D. KEENAN

Bureau of Meteorology Research Centre, Melbourne, Victoria, Australia

PAUL E. JOHNSTON

Cooperative Institute for Research in Environmental Sciences, University of Colorado, Boulder, Colorado

(Manuscript received 17 April 2000, in final form 28 February 2001)

ABSTRACT

This paper describes the results of an experiment that combines the data from a 5-cm-wavelength polarimetric radar and multiple-frequency wind profilers to examine the polarimetric signatures associated with the microphysical structure of several relatively shallow thunderstorms and also to examine quantitative rainfall measurements made with the polarimetric radar. These shallow storms produce considerable amounts of centimeter-sized hail. The presence and size of this hail are deduced from the wind profiler data. The melting hail particles produce a distinctive polarimetric signature with large values of differential reflectivity Z_{DR} and suppressed values of the correlation coefficient between the signals at horizontal and vertical polarization. Comparisons between the mass-weighted mean drop diameter and differential reflectivity have been performed and show reasonable agreement with theoretical expectations, although the observed Z_{DR} are somewhat smaller than expected. This may be associated with the theoretical assumption of the Pruppacher–Beard oblateness relationship even though there is evidence to suggest that real raindrops may be less oblate on average in convective rain. Quantitative polarimetric rainfall estimators have been compared with rainfall rates derived from the profiler drop size distribution retrievals and show reasonably good agreement when reflectivity values are matched.

1. Introduction

Polarimetric radars offer significant potential for both quantitative measurement of rainfall and the objective classification of precipitation state (Zrnić and Ryzhkov 1999). There have been numerous studies using 10-cm-wavelength radars but relatively few with 5-cm radars. There are, however, some advantages in using 5-cm-wavelength radars. For example, for a given rain rate the specific differential phase K_{DP} is about 2 times that for a 10-cm-wavelength measurement (e.g., Sachidananda and Zrnić 1986), and indeed very good agreement has been observed between rain gauge measurements and K_{DP}-based rainfall estimates (May et al. 1999b). However, attenuation and differential attenuation are both much more significant issues with the smaller-wavelength measurement (e.g., Jameson 1991). The situation with respect to the classification of precipitation type is also at a much earlier stage of development than for 10-cm-wavelength measurements. In situ measurements within convective systems are very difficult, but techniques combining remote sensors offer the possibility of characterization and verification of precipitation type.

An ambitious experiment using 920- and 50-MHz wind profiler radars combined with 5-cm-wavelength polarimetric radar data was undertaken in Darwin, northern Australia, during the 1997/98 wet season. The profiler scans were coordinated in time and height sampling. The polarimetric radar (Keenan et al. 1998) was located 23 km from the profilers (Fig. 1). The key elements of the observation strategy were a radar scan sequence that included a range–height indicator (RHI) scan directed over the profilers, followed by a fixed-elevation/azimuth scan lasting 2 min at an altitude about

Corresponding author address: P. T. May, BMRC, GPO Box 1289K, Melbourne, 3001, Victoria, Australia.
E-mail: p.may@bom.gov.au

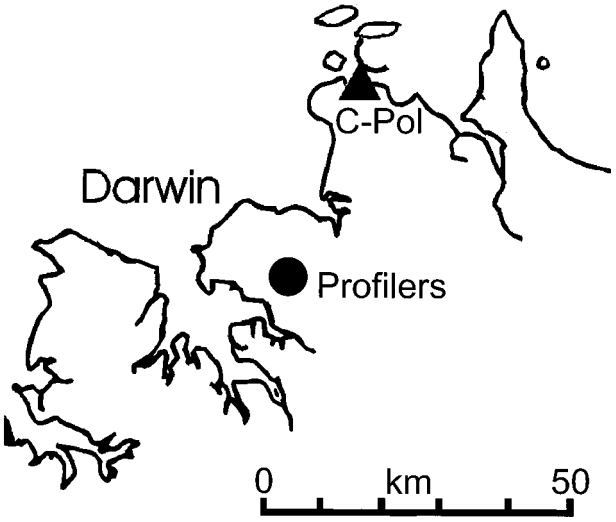

FIG. 1. Map showing the relative locations of the C-Pol radar and the profiler site.

2.5 km above the profilers to allow extended time series of polarimetric variables over the profiler and the possibility of similar temporal averaging. The profiler scans focused on the vertical beam (45 s out of every 1 min), and the temporal and height sampling of the two profilers were matched to minimize errors associated with temporal and spatial variations of the vertical motion and microphysics in convective systems.

The combined profiler data not only allow a detailed examination of the vertical motion and precipitation microphysics of several short-lived storms that developed on sea-breeze fronts over the profilers, they also permit the deconvolution of particle size distributions at 45-s resolution. As a consequence, these observations can be used 1) to detect hail unambiguously, given that spectral peaks associated with hail occur at fall speeds far in excess of the maximum values for large rain drops and 2) to compute bulk parameters such as rainwater content and rainfall rate in still air when no hail is evident. Thus, the profilers provide independent estimates of bulk rain properties for comparison with the polarimetric radar observations. It is important that, with the profiler pulse volumes, a similar volume of air to that of the polarimetric radar is sampled. The fixed scan of the radar also allows data to be averaged over a similar time as the profiler data acquisition.

Data for such comparisons occurred in pure rain in only a few out of several tropical showers despite the echo tops only extending to about 2–3 km above the freezing level (~4.7–5 km). This paper presents some preliminary comparisons made between quantitative estimates of rain using polarimetric algorithms and those values computed independently from the profiler-deduced drop size distributions. Although data from this experiment yielded only a limited number of cases, such studies are valuable. The small number of cases is a result of the difficulty in obtaining cases directly over the profiler site. It is obvious from this study that ice plays a major role in even modest tropical showers extending only a few kilometers above the freezing level, as also was found in Florida summer showers during the Convection and Precipitation/Electrification experiment (e.g., Jameson et al. 1996), but the focus here is on the relationship between the polarimetric measurands and the microphysical characteristics of the precipitation.

2. Measurements

a. C-Pol radar

The Bureau of Meteorology Research Centre C-band polarimetric radar (C-Pol) is described in detail by Keenan et al. (1998). The important characteristics for this paper are that the radar is a 1°-beamwidth, 5-cm-wavelength radar located 23.6 km from the profiler site. The radar provides high-quality estimates of radar reflectivity factor at horizontal polarization Z_h, differential reflectivity (Seliga and Bringi 1976) Z_{DR}, accumulated differential phase shift Φ_{DP}, and the copolar cross correlation at zero lag $\rho_{hv}(0)$ (Mueller 1984; Jameson and Mueller 1985) measured using the algorithms described by Zahrai and Zrnić (1993) in real time. The high quality of the data is illustrated in Keenan et al. (1998) and May et al. (1999b). The range resolution of the observations was 150 m. The specific differential phase shift K_{DP} (range derivate of the propagation differential phase shift ϕ_{DP}) between vertical and horizontal polarizations has been estimated offline using all the successive Φ_{DP} estimates and the first derivative of a nonparametric local-regression monotonically increasing fit based on a variable number (>8) of points along the lines discussed in Jameson and Caylor (1994).

The scanning strategy employed for this experiment consists of a sequence of a volume scan followed by an RHI directed over the profiler site and a 120-s-long fixed-elevation scan over the profilers. The volume scan provides a description of the mesoscale organization of the storms, and the RHI scan provides the detailed height structure of the storms at the profiler site.

The fixed scan provides long time series of the radar variables over a period covering the profiler measurements and thus allows for direct comparison of the polarimetric measurements with the predicted estimates based on the profiler precipitation retrievals averaged over the same time. The polarimetric radar data were averaged in range and the profiler measurements in height to match the effective resolution volumes of the measurements as well as the sampling times.

b. Profiler observations

The experiment utilized two wind profilers, one operating at a frequency of 50 MHz and a second at a frequency of 920 MHz (Table 1). Both systems were sampling for 45 s in the vertical beginning at each mi-

TABLE 1. Operating parameters of the Darwin profilers (V is vertical; E is east; N is north).

Parameter	50-MHz profiler	920-MHz profiler
Scan sequence	V (45 s), E (15 s), V (45 s), N (15 s)	V (45 s), E (15 s), V (45 s), N (15 s)
Height resolution	315 m	105 m
Height coverage	1.5–20 km	200 m–12 km
Beamwidth	3°	9°

nute followed by 15 s on an off-vertical beam. This paper utilizes data only from the vertical beams. The 50-MHz system is used to measure the vertical wind speed and the spreading of the Doppler spectrum because it is less sensitive to precipitation than is the 920-MHz system. This spreading is associated with temporal variations in the vertical wind (the same for both profilers) and the finite beamwidth of the profilers. Although the beam broadening is greater for the 920-MHz system, the relatively low wind speeds in the Tropics (except in tropical cyclones) make this correction of only second order and only produces very small errors (Rajopadhyaya et al. 1998). The large temporal and spatial variability of the vertical motion in convection make beamwidth effects even less important in these data. The 920-MHz system is used as a vertically pointing Doppler weather radar to obtain reflectivity-weighted fall speed spectra. Of course, this means that the 920-MHz system must be calibrated (see appendix A) and the precipitation retrievals must handle the presence of some clear-air echoes. The spatial size of the drafts is large enough when combined with the equivalent time averaging of the profiler data that there is little difference between the vertical motion sampled by the two profilers.

Although the observations of vertical motion date to the earliest profiler applications, precipitation retrievals warrant additional discussion. Weather radars have been operated in a vertically pointing mode to retrieve drop size distributions (DSD) in precipitating clouds (e.g., Rogers 1967; Atlas et al. 1973), but these studies demonstrated potentially large errors induced in the procedure because the vertical air motions could not be measured directly. The use of profilers to measure simultaneously the vertical motion and the reflectivity-weighted fall speed spectrum allowed the application of rain DSD retrievals (e.g., Wakasugi et al. 1986; Gossard 1988). The reflectivity-weighted fall speed spectrum, corrected for mean vertical motion and turbulent/shear spectral broadening, is then used to estimate DSD using a fall speed–drop diameter relation. These profiler retrievals can be performed directly without boundary condition or uniform echo coverage assumptions and can operate with minimum attention for long periods of time (Sato et al. 1990). Single-frequency retrievals (as described above) were often limited by certain types of rain conditions because of the large differences between the clear-air and precipitation echo strength at the various profiler frequencies. Because the 50-MHz systems are less sensitive to precipitation, separation of the precipitation peak from the clear-air peak can be difficult, especially with drizzle or snow. This motivated the development of dual-frequency techniques utilizing the 50-MHz vertical motion estimates and the 920-MHz profiler's sensitivity to precipitation echoes (Currier et al. 1992; Maguire and Avery 1994). These dual-frequency retrievals are more accurate and can be performed under almost all rain conditions (Rajopadhyaya et al. 1999). Moreover, the short decorrelation time of the signals at the higher frequency allows more independent samples in a given time. This in turn allows higher time resolution. It is only possible to do these retrievals in active convection using dual-frequency methods because the rapid variations in vertical wind overhead require high time resolution.

Before discussing the retrieval process, it is useful to examine some examples of the Doppler spectra. Figure 2 shows three sets of Doppler spectra. The first was taken in the decay phase of a storm in which the vertical velocity was weak and the turbulence was low. Thus, the 50-MHz spectrum is narrow. The 920-MHz precipitation echo is much broader and is asymmetric, indicating that the broadening due to turbulence and beam broadening is of second order (cf. Rajopadhyaya et al. 1998) and the spectrum contains considerable information on the DSD. A small clear-air peak is also visible at the same velocity as the 50-MHz spectrum. The second case is pure rain in convection, and the clear-air spectra are much broader, indicating some of the difficulties to be faced in precipitation retrievals. The noisy nature of the 50-MHz spectrum is a function of the small number of independent spectra that have been accumulated and averaged in 45 s. Note the relative smoothness of the 920-MHz spectrum that still allows an accurate retrieval, although the corrections for broadening are now important. The third case is also in convection, but the 920-MHz spectrum is clearly multimodal. Furthermore, the high-velocity peak is at fall speeds beyond the asymptotic limit for rain ($\sim$10 m s^{-1}; e.g., Atlas et al. 1973) indicating the presence of hail. The fall speed of about 12 m s^{-1} is consistent with hail that has a diameter of about 15 mm (Houze 1993). In clear examples such as this one, it is possible to retrieve both rain and hail size distributions, but, as will be seen in some later examples, it is often clear that there is a hail–rain mixture but there is little spectral separation.

If $P(v)$ is the reflectivity-weighted fall speed spectrum and $G(v)$ is the clear-air spectrum, the observed Doppler spectrum $S(v)$ is given by

$$S(v) = P(v) \otimes G(v) + G(v) + N, \qquad (1)$$

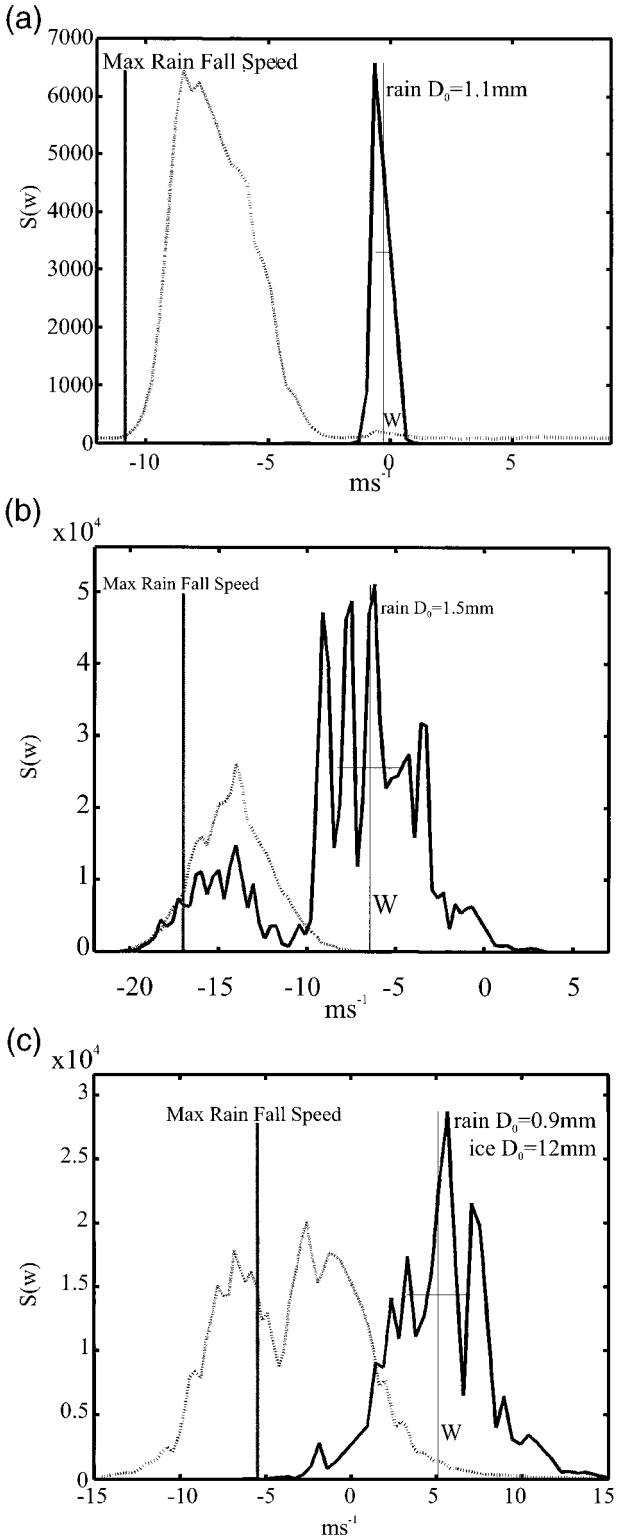

where $P(v)$ is the reflectivity-weighted fall speed spectrum, $G(v)$ is the clear-air spectrum, $\otimes$ represents a convolution, and N is the noise level. There are two approaches to obtaining $P(v)$. One is to assume some functional form for P and to use a least squares approach to fit the model spectrum to S, where G is measured either from the same spectrum (Wakasugi et al. 1986) or from a 50-MHz profiler (Currier et al. 1992). The alternative approach is to fit a Gaussian curve to G and then to deconvolve S to obtain an estimate of P (e.g., Gossard 1988). We use the latter except, again, the estimate of G is taken from the 50-MHz measurements. Potential problems arise with the deconvolution because a complete deconvolution is impossible in the presence of noise. An iterative approximation is used here (cf. Gossard 1988). Once P is obtained, a simple change of variables is used to obtain the DSD. For example, for rain the fall speed relation of Atlas et al. (1973) can be used:

$$w = (9.65 - 10.3e^{-0.6D})(\rho/\rho_0)^{-0.45}, \quad (2)$$

where w is the fall speed in still air (m s^{-1}), D is the diameter (mm), ρ is the air density, and ρ_0 is the air density at mean sea level pressure. Note that the fall speed relation gives an asymptotic limit for the maximum rain fall speed at mean sea level pressure of 9.65 m s^{-1}. There are numerous examples in the data for which there is considerable energy and even clear peaks at speeds in excess of this limit, showing the presence of hail (e.g., Fig. 2c). Using a hail fall speed relation (Houze 1993),

$$w = 1.426D^{0.8}(\rho/\rho_0)^{-0.45}, \quad (3)$$

particles with fall speeds in the range of 11–14 m s^{-1} at a height of 2.5 km correspond to diameters of 10–15 mm.

Limitations of the profiler retrievals of rain include a minimum observable diameter of about 0.7 mm because of the weak scatter from such small drops and potential contamination by clear-air scatter and the smearing of drops greater than about 4 mm into a single spectral frequency bin as the diameter–fall speed relation moves asymptotically to a constant fall speed for very large drops. Thus, the profiler spectra cannot be used to discriminate a few very large drops that may have significant impact on the polarimetric variables (Keenan et al. 2001). However, the results of modeling

←

FIG. 2. Examples of the 50-MHz (solid) and 920-MHz (dotted) Doppler spectra for (a) stratiform rain, (b) convective rain, and (c) rain–hail mixture. The vertical line with the 50-MHz spectra marks the vertical velocity estimate, and the line with the 920-MHz spectrum marks the asymptotic limit for rain fall speeds (particles falling faster than this are hail). Note that there is some spectral broadening due to turbulence and finite beamwidth, so the extension of the spectrum in (b) to hail fall speeds is not significant. These spectra are not calibrated, so the units are arbitrary.

studies (e.g., Rajopadhyaya et al. 1993, 1999), comparisons of rain rate measurements (Rajopadhyaya et al. 1998; Cifelli et al. 2000), and in situ measurements (Rogers et al. 1993) all indicate that the accuracy of the retrieved DSDs is good. In particular, the rain rates measured by gauges and profiler retrievals in convection were highly correlated and within about 20% (Rajopadhyaya et al. 1998).

c. Matching sample volumes

The 920-MHz profiler is looking vertically and has a 9° beamwidth. Therefore, the pulse volume at a height of 2.5 km is approximately a disk 105 m thick with a diameter of about 400 m. The polarimetric radar has a range resolution of 150 m, has a beamwidth of 1°, and is located 23.6 km from the profiler site. Therefore, the C-Pol pulse volume is approximately a disk perpendicular to the profiler volume with a depth (diameter) of 500 m and is 150 m thick. Note that for the fixed-elevation scan there is no smearing of the pulse volume by the antenna movement. For the RHI scans, the volume is smeared in the vertical with sampling about every 0.7° as the beam is scanned. The resulting smearing is small and increases the vertical extent of the pulse volume by about 100 m. Thus the sampling volume can be matched well by averaging the 920-MHz profiler data over five range gates and the C-Pol data over three range gates about a location as close to the center of the common volume as possible. This matching has been used to calibrate the profiler reflectivities (appendix A) and for comparing the polarimetric signatures to profiler data.

3. Two examples of the storms

Prior to discussion of the relationships between the polarimetric radar observations and the derived microphysical properties of the precipitation within the common sample volumes measured with the profilers, it is useful to describe briefly the storms in question. Thus, time–height cross sections of the profiler-derived radar reflectivity are shown for two storms (Fig. 3). These show storm tops of about 7 km, extending only about 2 km above the freezing level. These storms were generally short lived, with lifetimes of less than 1 h, but had rapid development as the convection started. The peak reflectivity within the cells reached values in excess of 55 dBZ (Fig. 3a, 0410–0435 UTC; Fig. 3b, 2330 UTC), and this was usually reached within 10 min of the first echoes exceeding 30 dBZ. Despite the relatively shallow nature of the cells, we will show that these storms typically contained significant amounts of hail extending down as low as 2–3 km above the ground, consistent with results from Braham (1964) and Jameson et al. (1996). These storms contained large updraft intensities (>10 m s^{-1}) on the periphery of the cells and large-amplitude descending motion in the central part of the core (Fig. 3a, ~0430 UTC; Fig. 3b, ~2337 UTC). The updraft magnitudes were sufficient to loft even the largest drops above the freezing level, allowing the efficient production of large hail particles. Near the cell center where there are no strong upward velocities, and when the cells are decaying, the profiler and polarimetric signatures are consistent with pure rain at heights near 2.5 km. The meteorological conditions of these storms are discussed in more detail in May et al. (1999a).

Figures 4 and 5 are panels of the C-Pol data collected 2.5 km above the profilers as the antenna remained stationary. In Fig. 4 corresponding to yearday (DOY) 330 (26 November 1997), some precipitation lay between the radar and the profiler site, leading to some attenuation. This is accounted for as indicated (see appendix B for details). Figure 5 corresponds to data collected on DOY 345 (11 December 1997). There was no significant intervening attenuation observed on DOY 345, as illustrated by the small values of the range-integrated K_{DP} (i.e., Φ_{DP} with backscatter phase jumps removed). In the beginning of the data for DOY 330, there is clear evidence [i.e., the simultaneous appearance of larger Z_{DR} and values of $\rho_{hv}(0)$ suppressed significantly below those typical of rain (see Jameson 1989)] of some residual hail as confirmed by the profiler observations. This is discussed in detail in section 5. For DOY 330, the profiler DSD measurements were made from 17 to 62 s. Thus, to some extent they likely included some effects due to melting hail, at least initially. On DOY 345, however, the profiler measurements were over the period of 14–59 s when no hail was present.

4. Relations between drop diameter and differential reflectivity

T-matrix scattering calculations have been used to obtain an estimate of the relation between parameterizations of the DSDs and the polarimetric measurands (e.g., Aydin and Giridhar 1992). These have usually assumed that the DSDs have the form of a gamma distribution, and the actual coefficients have been estimated from fits to disdrometer data collected at the ground. The dataset here presents an opportunity to compare the polarimetric data and the profiler retrievals of the DSDs, sampling common volumes. To obtain as clean a comparison as possible, the 920-MHz profiler data and the polarimetric radar data have been averaged in range as described in 2c, and the C-Pol data have been averaged over the profiler sampling time to match the sampling volume and temporal sampling as closely as possible.

The DSDs are parameterized by the mass-weighted median diameter given by the ratio of the fourth and third moments of the DSD:

$$D_m = \int D^4 N(D)\, dD \Big/ \int D^3 N(D)\, dD. \qquad (4)$$

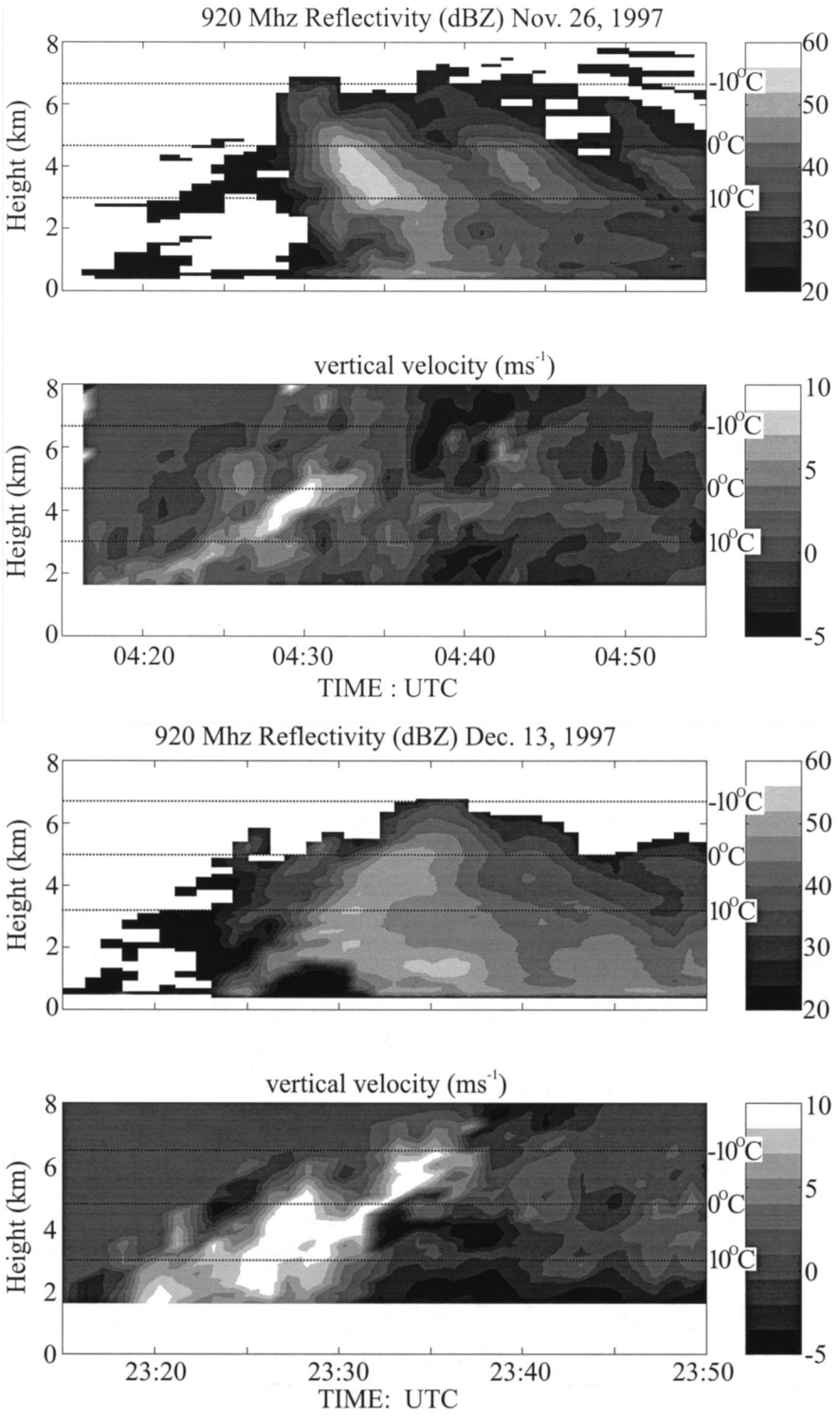

FIG. 3. Time–height cross sections of the vertical velocity and reflectivity of two storms. The data to be discussed in detail are taken from these two examples, but similar results are obtained from other cases.

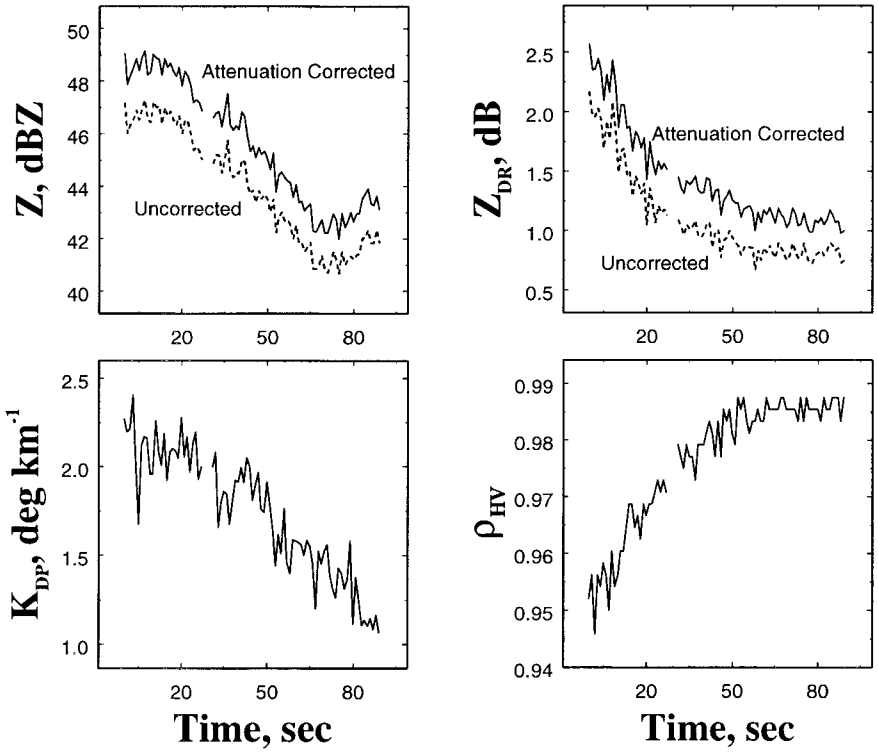

FIG. 4. C-Pol radar variables observed during 26 Nov 1997, 2.5 km above the radar profilers observing over the same volume and altitude. Here, K_{DP} is recomputed from the recorded integrated differential phase shift.

The variable D_m is closely related to the often-used median volume diameter (D_0: diameter such that 1/2 of the water mass lies at a diameter above D_0) but in general is slightly larger; D_m is used here because it arises naturally in scattering calculations (e.g., Jameson 1994).

Figure 6 shows a scatterplot of the observed values of D_m measured with the profilers against the C-Pol estimates of Z_{DR} along with the theoretical relation (using linear Z_{DR}: $\zeta = 10^{Z_{DR}/10}$) and model results derived in a manner similar to that of Jameson (1994). The different large symbols denote measurements on different days. Note the cluster of Z_{DR} values between 0.5 and 1 dB with diameters above where theory suggests. The offset is not due to biases induced by the artificial truncation of the DSDs at diameters below 0.7 mm. For exponential distributions, this truncation causes a bias of about 0.1 mm, which is clearly insufficient to bring the observations into agreement with theory. This is probably an overestimate of the bias, because the data suggest that the DSDs have some curvature, indicating fewer very small drops as compared with an exponential distribution. The discrepancy may be associated with the theoretical assumption of the Pruppacher equilibrium oblateness relation (Pruppacher and Beard 1970); recent evidence suggests that real raindrops may be less oblate on average in convective rain (Beard et al. 1989; Andsager et al. 1999; Keenan et al. 2001).

The overall impression of the observations is a flatter distribution than the theoretical curve. However, there are a number of points at which the profiler data indicate the presence of significant amounts of hail. These are the points at which the Z_{DR} values are greater than 2 dB and are below the theoretical line. Note that for tumbling hail the Z_{DR} tends to 0 dB. However, as drops melt, there is evidence that drops with large hail cores may have considerable oblateness (Chong and Chen 1974). This is explored further in section 5. There is another outlying point with a D_m of about 1 mm but large Z_{DR}. However, this point was obtained for a sample on the edge of a storm, so any pulse volume mismatch may be a significant factor in this difference.

5. Hail–rain mixture signatures

As noted earlier, the profiler data show unambiguous detection of hail with fall speeds greater than 12 m s^{-1}, most likely frozen drops with a diameter of about 10 mm. These are present several kilometers below the freezing level and will clearly be water coated. This raises the obvious question of what polarimetric radar signatures accompany the melting. With large hail, the ice is tumbling, with the effect of producing very low values of Z_{DR}. However, there is good laboratory evidence to suggest very different behavior with these smaller particles. As frozen pellets melted in a wind tunnel, they stopped tumbling, became oriented hori-

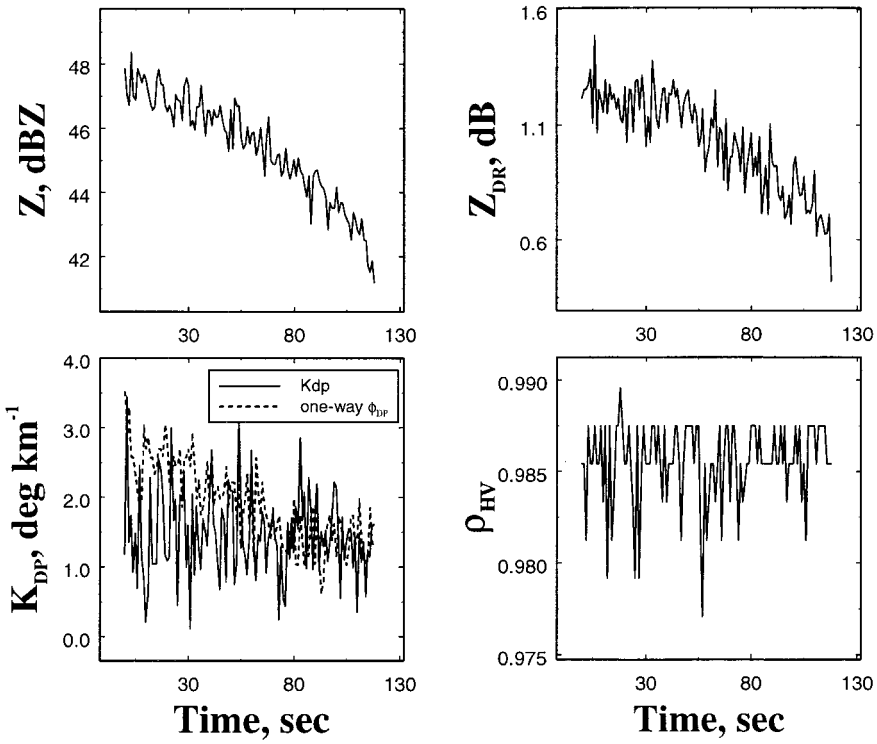

FIG. 5. Same as Fig. 4 but for 11 Dec 1997. Because there was no intervening precipitation, attenuation correction was not necessary.

zontally, and developed a ring of water so that the particles have considerable oblateness (Blanchard 1950; Chong and Chen 1974). These data offer the opportunity to test if such signatures are seen in real rain. There are several examples of both pure rain and rain mixed with melted frozen drops. Two of the clearest examples will be shown, although the other cases are all consistent.

An example of pure rain is shown first and will serve to provide a contrast to an example with significant hail. Figure 7 shows a panel with profiles of the polarimetric variables along with the reflectivity-weighted fall speed spectra relative to the air (i.e., the vertical motion has been subtracted), observed with the 920-MHz wind profiler and the asymptotic limit for rain terminal fall speeds. Figure 7a is for a case with pure rain. Despite the presence of large drops, as indicated by the fall speed spectra peaking near the asymptotic limit but with no significant energy at fall speeds beyond, the values of Z_{DR} are modest and the $\rho_{hv}(0)$ remain high (>0.97). The distributions of these variables at a particular height in the storm are all very narrow, as shown in histograms of the measurements within ± 1 km of the profiler range (Fig. 8a). These pure rain cases tended to occur in the downdraft parts of the storm or when there is weak vertical motion. Note that there is broadening of these spectra by turbulence and beamwidth effects. This produces some spectral power with apparent upward falling drops but does not change the conclusions drawn in the paper.

The profiles when melting hail is present (Figs. 7b and 8b) are very different. At the upper heights, the Z_{DR} is low, the $\rho_{hv}(0)$ is high, and the distributions are narrow. As the hail descends, there is a rapid increase in Z_{DR} and corresponding decreases in $\rho_{hv}(0)$. The distributions become extremely wide. There is evidence at the lowest heights that, as the drops completely melt, the distributions narrow and more typical values of Z_{DR} and $\rho_{hv}(0)$ are found. These data tend to occur in large updrafts so that the only particles with fall speeds sufficient not to be lofted are hail. The small fall speeds at the upper height correspond to low reflectivities and probably small particles at this time. Larger hail is also found aloft at other times. Note that the size of the melting hail is such that resonance effects are important.

There is also a corresponding increase in the values of K_{DP} as the hail melts. This may produce errors in the polarimetric rain measurements, but will be partially compensated by the fact that the hail density is high so that the high values of K_{DP} are indeed representing regions of high water content and in a sense real large drops. Large drops do have a significant effect on the appropriate rain rate–K_{DP} relationship (e.g., Keenan et al. 2001). These effects were not apparent in the data examined by May et al. (1999b) because the data examined there were mostly from below a height of 1 km.

A possible alternative explanation for these polarimetric signatures is the presence of large water drops causing resonance effects. Resonance effects are high-

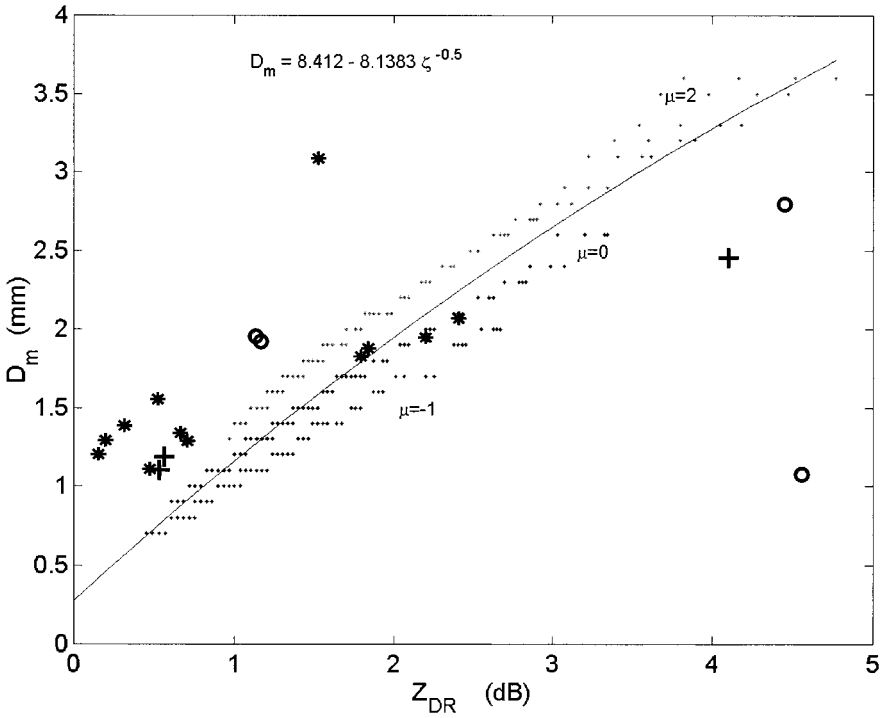

FIG. 6. A scatterplot of the differential reflectivity Z_{DR} against the mass-weighted median drop diameter of the drop size distributions D_m. The dots are from simulations using assumed gamma DSDs; the *, ○, and + represent observed data using C-Pol estimates of Z_{DR} and D_m obtained from profiler retrievals of the DSD on various days. The curve represents a fit to the model data as an algorithm for estimating the mass-weighted drop size using attenuation-corrected Z_{DR} in linear units (ζ) at 5.48 GHz.

lighted in simulations with monodisperse distributions, but in realistic DSDs the effects are much less obvious because the positive and negative peaks tend to wash each other out (e.g., Keenan et al. 2001), but the extremes of the polarimetric measurands do extend to a population near the observations here. However, the hail signatures were seen in every storm and were correlated with hail detections in the profiler data, supporting the melting-hail hypothesis.

The observed polarimetric characteristics during the melting of the frozen drops are in a different parameter space in precipitation classification schemes when compared with those tuned for large hail that tumbles and mixed rain and graupel but are consistent with the expectations from the wind tunnel data of melting hail with diameters of about 1 cm (e.g., Chong and Chen 1974; Rasmussen et al. 1984) and modeling based on these data (Vivekanandan et al. 1990). The Vivekanandan et al. (1990) results also showed enhancements in the Z_{DR}, and so on, of a magnitude similar to these observations and at a similar distance below the freezing level, although their model results neglected vertical velocity, which is clearly important. A part of this difference may arise because of the sensitivity of melting rates to the humidity profile (Johnson and Jameson 1982). Particles falling through a dry environment remain frozen longer than those falling through a moist environment because of the cooling when the water evaporates.

6. Quantitative rainfall estimates in rain

There are many variables to compare, but the number of ''pure rain'' cases is so limited that in this paper we only consider the algorithms for the rainfall rate as described in section 2 and appendix B as an illustration of the kind of studies possible with a much larger set of data. It is important to remember that the radar and profilers are looking over the same volume so that this comparison avoids any effects due to evaporation, advection, or dispersion such as occur when comparing radar observations with rain gauge and ground-based disdrometer observations. In addition, vertical air velocity no longer plays a role. Again we will examine two cases, this time utilizing the 2-min fixed-elevation/azimuth samples. The first was taken when the profiler data indicated there was pure rain present for the whole record, whereas for the second there was some hail present in the first part of the record but not as much as for the cases discussed in the previous two sections. There was no hail for the profiler record that is completely enclosed within the radar sample time. These examples should also be representative of the performance of the polarimetric estimators at lower elevations.

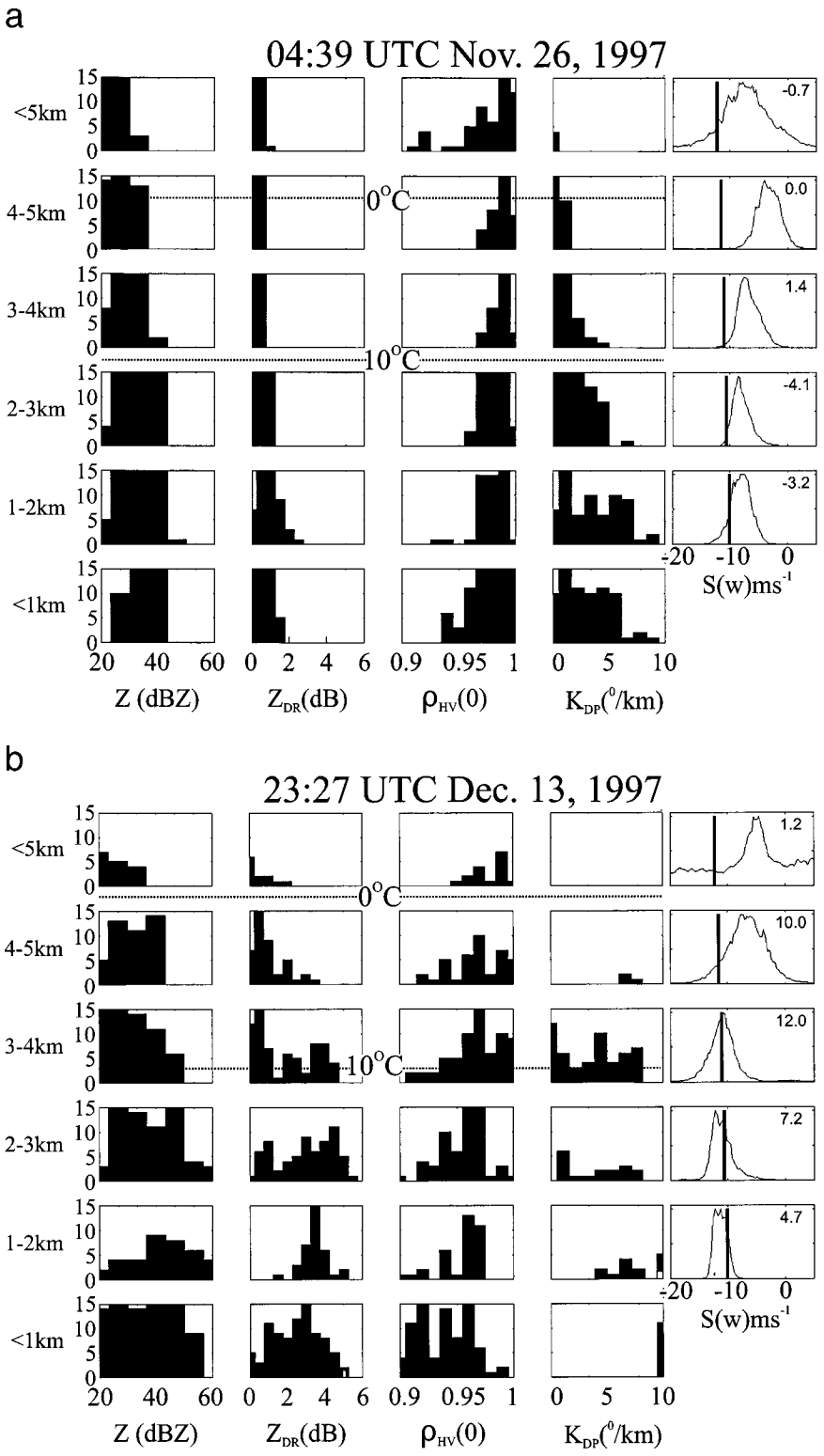

FIG. 7. Height profiles of the polarimetric variables near the profiler site together with examples of the reflectivity-weighted fall speed spectra measured with the profilers at the corresponding heights. The mean vertical motion has been subtracted, and the vertical line marks the asymptotic limit for fall speeds of very large raindrops; (a) pure rain example; (b) example when hail is detected, as seen by the significant spectral energy at speeds beyond those for rain. The vertical velocity (m s^{-1}) is given next to the spectra.

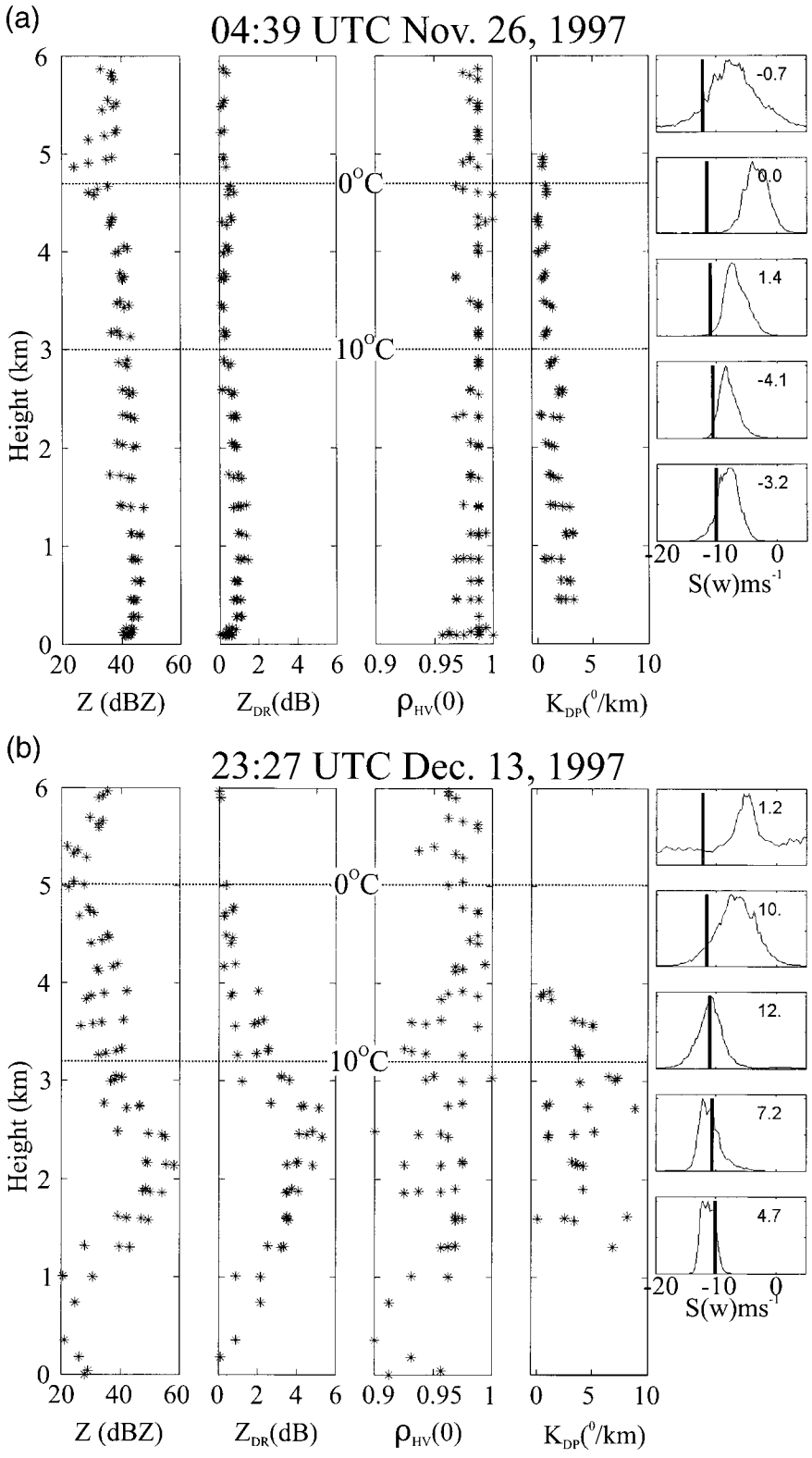

FIG. 8. Histograms of the polarimetric variables as a function of height within a range of ±1 km of the profiler site: (a) pure rain, (b) hail present.

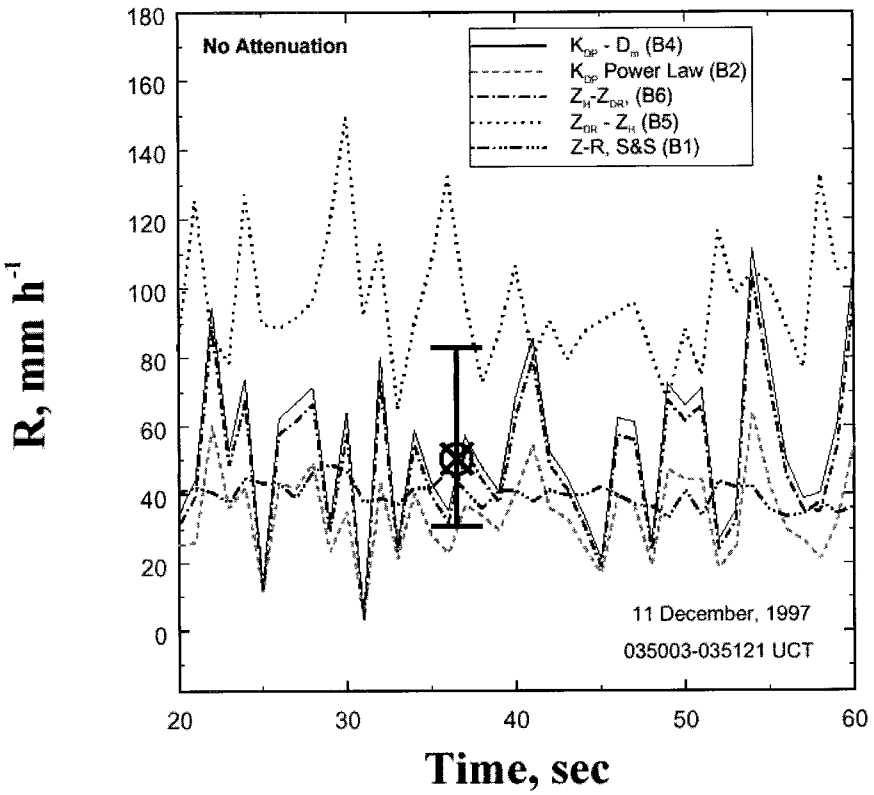

FIG. 9. A comparison between the C-Pol estimates of rainfall rate and the value (circled cross) calculated from the profiler-derived DSDs for a sample on 11 Dec 1997. The various radar algorithms in the legend are discussed in the text. The capped bar denotes the estimated uncertainty from the calibration of the profilers.

Time series of a number of radar-based estimators using both single and multiparameter estimators as described in appendix B are shown in Figs. 9 and 10. The profiler estimates of rainfall rate calculated from the DSD estimates are also shown, with the main contributor to the uncertainty being the radar calibration. Even with the careful intercalibration of the radar, there are significant differences in the individual reflectivity estimates. This in part illustrates the well-known difficulty of quantitatively comparing radar estimates on very short timescales. For the purposes of this section, we avoid this source of discrepancy by using the DSD shapes measured by the profiler retrievals but with the total concentration being determined using the C-Pol reflectivity. Data have been selected for a pure rain case and a case in which there is some hail contamination in the early part of the record.

Data for a sample on 11 December 1997 show that all the estimators (appendix B) except for the Z–Z_{DR} estimate agree very well in the early part of the record. The estimators utilizing Z_{DR} show larger fluctuations, indicating contributions from the statistical measurement errors in Z_{DR}. This has lead Fulton et al. (1999) to propose averaging the Z_{DR} estimates over a larger area. The estimates with a Z_{DR} component also increase at the end of the record. One-minute-resolution rain rates calculated from disdrometer data collected at the profiler site with a time correction to allow for the rain to reach the ground show very good agreement with the simple estimators, with rates of 36 mm h^{-1} for the early part of the record, decreasing to 23 mm h^{-1} by the end. The time delay was estimated independently using the sloping reflectivity shafts in the profiler reflectivity data.

The situation for the record taken during 26 November is more complicated. The profiler data overlapping the first 30 s of the record show hail echoes with a magnitude within 2 dBZ of the rain echo. In the next profiler sample, which was taken from within the C-Pol sampling interval, the hail had decreased to more than 10 dBZ below the rain intensity and can be ignored. Of interest, the various estimators agree more closely when the hail was present, whereas the Z_{DR}-based estimators (except for K_{DP}–D_m) tended to overestimate the rain rates for the pure rain, where again disdrometer data verify the magnitude and the time evolution of the Z–R and R–K_{DP} estimators closely (44 mm h^{-1} early, decreasing to 28 mm h^{-1}). In Fig. 10, it is specifically apparent that those algorithms using K_{DP} and the Z–R relation do better than those using Z_{DR}, perhaps because Z_{DR} is underestimated because of insufficient compensation for differential attenuation. The good agreement in the early part of the record may be somewhat for-

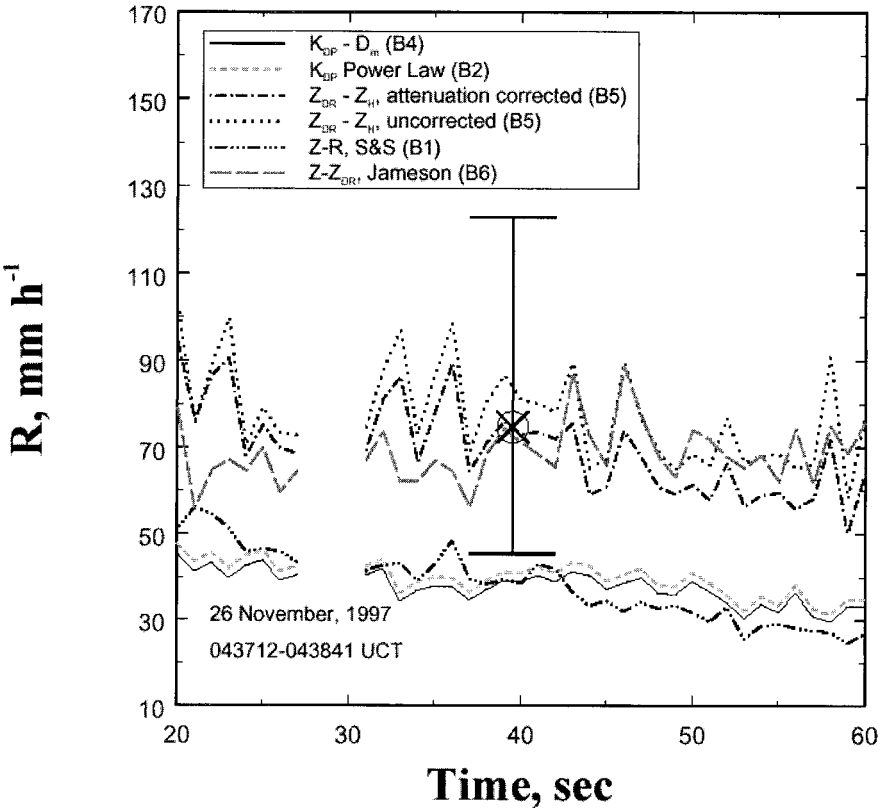

FIG. 10. Same as Fig. 9 but for 26 Nov 1997.

tuitous because of the enhanced Z_{DR} effects discussed in the earlier sections.

7. Concluding comments

Although it is obvious that no global conclusions are possible from the limited set of examples from this experiment, it is clear that a long-term study of this kind (preferably initially at nonattenuating frequencies) could begin to provide definitive and useful comparisons among radar polarization algorithms without many of the afflictions associated with comparison with ground-based measurements. These usually involve instruments with vastly different sampling volumes that severely influence such comparisons (Jameson and Kostinski 2001; Kostinski and Jameson 2000). This applies not only to the rainfall rate but also to other rainfall parameters. However, these preliminary results using data with similar sampling are very encouraging, particularly the K_{DP} and combined K_{DP}–Z_{DR} estimators at high rainfall rates and conventional Z and Z–Z_{DR} estimators at low rainfall rates.

All the tropical storms examined in this study contained copious amounts of hail despite the tops only extending to 2–3 km above the freezing level. The hail signatures were seen in both the profiler data and the polarimetric radar data. Large hail has been found in similar storms in Florida (e.g., Braham 1964), and more recently significant ice has been found in many locations (e.g., Jameson et al. 1996; Carey and Rutledge 2000). This ice is associated with the large-amplitude vertical motions that were found on the outer sides of the cells. The results show very clearly the potential impact of melting hail, with exaggerated values of Z_{DR} and $\rho_{hv}(0)$. These exaggerated values have considerable impact on precipitation classification schemes and quantitative rainfall estimation using a number of remote sensing techniques. Furthermore, they result in vertically erect columns of enhanced Z_{DR} as have been observed in many intense storms and have generally been interpreted as an indication that very large drops are present. Even in tropical showers with a high freezing level, this interpretation may be erroneous. These observations clearly show that at least some Z_{DR} columns are associated with melting hail and the stabilization of large drops by the hail cores.

Acknowledgments. A. R. Jameson was supported for this research by grants from the National Science Foundation's Physical Meteorology Program (Dr. Ron Taylor, retired) under Grant ATM-9419523. The 920-MHz wind profiler used in this study is supported by the NOAA Aeronomy Laboratory. The disdrometer data were sup-

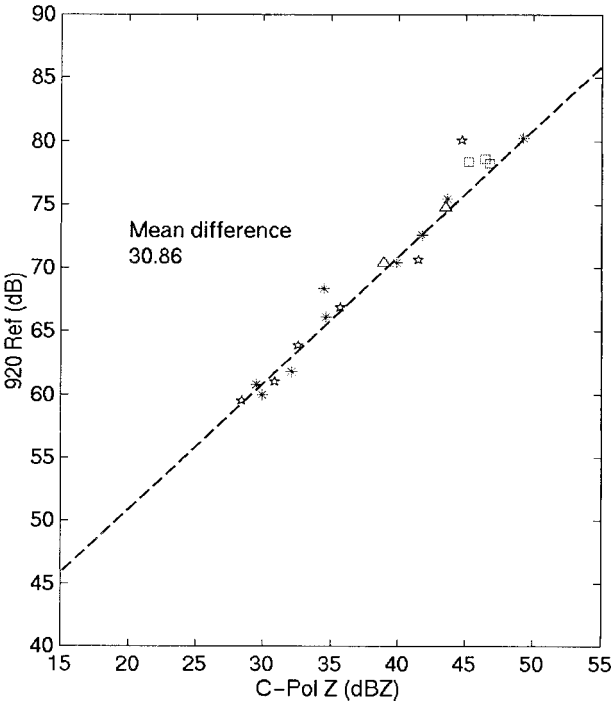

FIG. A1. Cross calibration of the reflectivities measured with the C-Pol radar and the 920-MHz wind profiler echo power with a range-squared correction. Their respective sampling volumes have been averaged to an approximately common volume (see text for details). The mean offset of 31.8 dB provides a calibration factor for the profiler.

plied by M. Maki of National Research Institute for Earth Science and Disaster Prevention, Japan.

APPENDIX A

Intercalibration of the Radars

Calibration of weather radars, and vertically pointing ones in particular, is notoriously difficult. The C-Pol radar has been calibrated using a solar calibration and careful hardware checks. The extended constant-elevation scan offers an opportunity to calibrate the 920-MHz system absolutely. The aim was to make use of the common sampling in time and a close match of the respective radar volumes with some range averaging of both the C-Pol and 920-MHz profiler data. The C-Pol data have had attenuation corrections using the observed range integrated K_{DP} (Φ_{DP} without backscatter phase jumps) and a theoretical attenuation–K_{DP} coefficient (Bringi et al. 1990; Keenan et al. 2001).

A scatterplot of the reflectivity measurements using data selected over several days is shown in Fig. A1. The mean difference between the calibrated C-Pol reflectivity and the returned power observed with the profiler is 31.8 dB. An alternative is to use a least squares fit of a straight line to the data; a slope of about 0.9 is obtained. However, the variance about such a fit and a simple $y = x - 31.8$ line is not significant. Overall, the scatter about the linear dependence is only about ± 2 dB. The resulting estimated error of the mean is less than 0.5 dBZ. This agreement is impressive, but for individual quantitative rain estimates there is still the uncertainty of 2–3 dB, which represents a factor of 2 or more for water volume and rain rate. The variations are more than what is expected purely from random statistical errors in the reflectivity measurements themselves and so are probably related to residual pulse volume mismatches. These are particularly important in regions with large spatial and temporal variations.

APPENDIX B

Polarimetric Radar Algorithms

The suite of algorithms that relates the polarimetric measurables to drop size distributions and rainfall rates is presented below for different categories. In all cases, R is in millimeters per hour, K_{DP} is in degrees per kilometer, Z_H is in millimeters to the sixth power per cubic meter, Z_{DR} is in decibels, and A_H and A_{H-V} are in decibels per kilometer.

The focus for this paper is on using polarimetric radar estimates of rain and precipitation characteristics. Polarimetry has well-documented advantages over simple reflectivity-based estimates. For example, K_{DP} rain-rate estimates are relatively insensitive to DSD and are immune to attenuation (Zrnić and Ryzhkov 1996), but the R–K_{DP} coefficient is strongly dependent on the assumed oblateness relation of the drops as a function of diameter (Keenan et al. 2001). Dual parameter estimates are also used here and are less sensitive to DSD and oblateness effects. The coefficients in this paper have been derived using the equilibrium oblateness relation of Pruppacher and Beard (1970). There is some question over the applicability of this relation as compared with relations indicating less-oblate large drops (Beard et al. 1989; Kubesh and Beard 1993; Andsager et al. 1999; Keenan et al. 2001). However, comparisons with rain gauges at different locations show varying results (e.g., Matrosov et al. 1999; May et al. 1999b), even with the same radar (Matrosov et al. 1999). The analyses in this paper utilize polarimetric-based attenuation corrections, but these corrections are small because there were no storms between the profiler site and C-Pol.

Rain-rate estimates are computed using a variety but finite number of the multitude of estimators available in the literature. These include simple Z–R and R–K_{DP} power laws by Sekhon and Srivastava (1971) and Jameson (1991) respectively:

$$Z = 300R^{1.35}, \quad \text{and} \quad R = 23.52K_{DP}^{0.856}. \qquad \text{(B1)}$$

Where needed, K_{DP} is used to ''correct'' for attenuation of both Z and Z_{DR} using the values in Jameson [1992, Eqs. (2) and (3)], corresponding to a temperature of 10°C, namely:

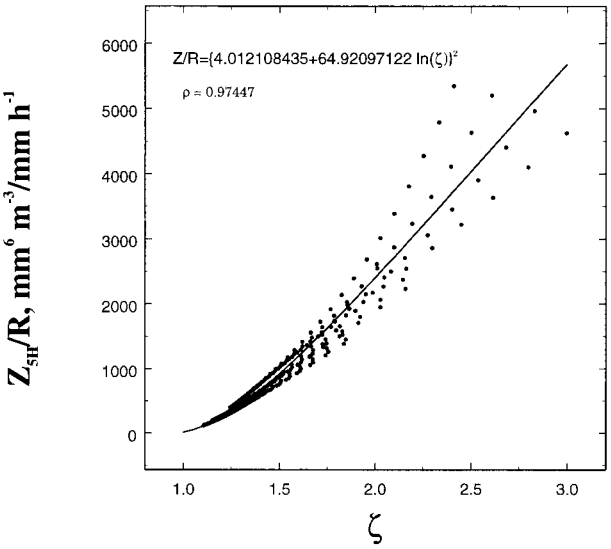

FIG. B1. An algorithm for estimating the rainfall rate using Z_H and linear Z_{DR} (ζ) at 5.48 GHz.

$$A_H = 8.108 \times 10^{-2} K_{DP}^{0.986}, \quad \text{and}$$
$$A_{H-V} = 1.436 \times 10^{-2} K_{DP}^{1.216}. \tag{B2}$$

There are a variety of relationships that have been published depending on the assumed oblateness and drop size distributions. These relationships are statistical in nature, and the most appropriate one seems to vary from case to case (e.g., Matrosov et al. 1999). The relations used here are based on a consistent set of simulations, although other relations may provide better fits to the data. Several dual-parameter estimates are also examined. These include combining the K_{DP} with the mass-weighted mean diameter D_m of the drop size distribution and Z–Z_{DR} estimates. The variable D_m is itself related to Z_{DR} ($\zeta = 10^{Z_{DR}/10}$) by the theoretical relations described in Fig. 6. The scatter occurs because of slight temperature effects and because the drop size distribution is a gamma distribution [$N(D) = ND^{\eta}e^{-\Lambda D}$] with the shape parameter η ranging over the set $\{-1, 0, 2\}$. The temperature is a relatively small effect, and distinctly separate curves are seen for the three values of the shape parameter. Recent profiler and disdrometer analyses favor the larger value of η as being more representative of the DSDs in convective rain. Then the relations from Table 1 in Jameson (1994) can be fitted to these data:

$$\frac{K_{DP}}{R} = 0.015\,463\,22 D_m^3 - 0.271\,550\,6 D_m^2 + 0.396\,224\,2 D_m - 0.017\,404\,15. \tag{B3}$$

There are two sets of Z_{DR}–Z_H relations. The first is illustrated in Fig. B1. The second is given by the relations given in Eq. (3), namely:

$$R = 2.6337 \times 10^{-3} Z_{DR}^{-1.1591} Z_H \qquad Z_{DR} \le 1.72 \text{ dB}$$
$$R = 4.586 \times 10^{-3} \zeta^{-3.625} Z_H \qquad Z_{DR} > 1.72 \text{ dB}$$
$$(\zeta > 1.486), \tag{B4}$$

from Jameson (1991, Table 2).

These relations have been developed using scattering calculations with assumed drop size distributions of pure rain. There are many cases in the datasets being analyzed for which there are clear signals in the profiler data of wet frozen drops with diameters of about 10 mm. Multiparameter radar measurements have proven to be a valuable tool in examining the microphysical processes within the mixed and ice phases of convective and stratiform clouds. For example, the combination of Z_{DR} and linear depolarization ratio measurements have been used to document the evolution of raindrop freezing and subsequent electrification process in Florida cumulonimbus clouds (Jameson et al. 1996). Moreover, the combination of Z_{DR} and ρ_{hv} (correlation coefficient) can serve as a proxy for the occurrence and size of hail in the radar volume (Balakrishnan and Zrnić 1990). The published relationships for hail assume that the scatters are tumbling, so their polarimetric signature is for low values of Z_{DR} and ρ_{hv}. However, for relatively small particles such as wet frozen drops, this may not be the case. This is explored further in section 5.

REFERENCES

Andsager, K., K. V. Beard, and N. F. Laird, 1999: Laboratory measurements of axis ratios for large raindrops. *J. Atmos. Sci.,* **56,** 2673–2683.

Atlas, D., R. C. Srivastava, and R. S. Sekhon, 1973: Doppler radar characteristics of precipitation at vertical incidence. *Rev. Geophys. Space Phys.,* **11,** 1–35.

Aydin, K. H., and V. Giridhar, 1992: C-band dual-polarization radar observables in rain. *J. Atmos. Oceanic Technol.,* **9,** 383–390.

Balakrishnan, N., and D. S. Zrnić, 1990: Estimation of rain and hail rates in mixed phase precipitation. *J. Atmos. Sci.,* **47,** 565–583.

Beard, K. V., H. T. Ochs, and R. J. Kubesh, 1989: Natural oscillations of small raindrops. *Nature,* **342,** 408–410.

Blanchard, D. C., 1950: The behavior of water drops at terminal velocity in air. *Trans. Amer. Geophys. Union,* **31,** 836–842.

Braham, R. R., Jr., 1964: What is the role of ice in summer rain-showers? *J. Atmos. Sci.,* **21,** 640–645.

Bringi, V. N., V. Chandrasekar, N. Balakrishnan, and D. S. Zrnić, 1990: An examination of propagation effects in rainfall on radar measurements at microwave frequencies. *J. Atmos. Oceanic Technol.,* **7,** 829–840.

Carey, L. D., and S. A. Rutledge, 2000: The relationship between precipitation and lightning in tropical island convection: A C-band polarimetric radar study. *Mon. Wea. Rev.,* **128,** 2687–2710.

Chong, S. L., and C. S. Chen, 1974: Water shells on ice pellets and hailstones. *J. Atmos. Sci.,* **31,** 1384–1391.

Cifelli, R., C. R. Williams, D. K. Rajopadhyaya, S. K. Avery, K. S. Gage, and P. T. May, 2000: Drop size distribution characteristics in tropical mesoscale convective systems. *J. Appl. Meteor.,* **39,** 760–777.

Currier, P. E., S. K. Avery, B. B. Balsley, K. S. Gage, and W. L. Ecklund, 1992: Combined use of 50 MHz and 915 MHz wind profilers in the estimation of raindrop size distributions. *Geophys. Res. Lett.,* **19,** 1017–1020.

Fulton, R. A., A. V. Ryzhkov, and D. S. Zrnić, 1999: Areal rainfall

estimation using conventional and polarimetric radar methods. Preprints, *29th Int. Conf. on Radar Meteorology*, Montreal, PQ, Canada, Amer. Meteor. Soc., 293–296.

Gossard, E. E., 1988: Measuring drop-size distributions in clouds with clear air sensing radar. *J. Atmos. Oceanic Technol.*, **5,** 640–649.

Houze, R. A., Jr., 1993: *Cloud Physics*, Academic Press, 573 pp.

Jameson, A. R., 1989: The interpretation and meteorological application of radar backscatter amplitude ratios at linear polarizations. *J. Atmos. Oceanic Technol.*, **6,** 908–919.

——, 1991: Polarization radar measurements in rain at 5 and 9 GHz. *J. Appl. Meteor.*, **30,** 1500–1513.

——, 1992: The effect of temperature on attenuation correction schemes in rain using polarization propagation differential phase shift. *J. Appl. Meteor.*, **31,** 1106–1118.

——, 1994: An alternative approach to estimating rainfall rate by radar using propagation differential phase shift. *J. Atmos. Oceanic Technol.*, **11,** 122–131.

——, and E. A. Mueller, 1985: Estimation of differential phase shift from sequential orthogonal linear polarization radar measurements. *J. Atmos. Oceanic Technol.*, **2,** 133–137.

——, and I. J. Caylor, 1994: A new approach to estimating rain water content by radar using propagation differential phase shift. *J. Atmos. Oceanic Technol.*, **11,** 311–322.

——, and A. B. Kostinski, 2001: What is a raindrop size distribution? *Bull. Amer. Meteor. Soc.*, **82,** 1169–1177.

——, M. J. Murphy, and E. P. Krider, 1996: Multiple parameter radar observations in isolated Florida thunderstorms during the onset of electrification. *J. Appl. Meteor.*, **35,** 343–354.

Johnson, D. B., and A. R. Jameson, 1982: On the melting of graupel and frozen raindrops. Preprints, *Conf. on Cloud Physics*, Chicago, IL, Amer. Meteor. Soc., 384–387.

Keenan, T. D., K. Glasson, F. Cummings, T. S. Bird, J. Keeler, and J. Lutz, 1998: The BMRC/NCAR C-band polarimetric (C-POL) radar system. *J. Atmos. Oceanic Technol.*, **15,** 871–886.

——, L. D. Carey, D. S. Zrnić, and P. T. May, 2001: Sensitivity of 5-cm wavelength polarimetric radar variables in rain to raindrop axial ratio and drop size distribution. *J. Appl. Meteor*, **40,** 526–545.

Kostinski, A. B., and A. R. Jameson, 2000: On the spatial distribution of cloud particles. *J. Atmos. Sci.*, **57,** 901–915.

Kubesh, R. J., and K. V. Beard, 1993: Laboratory measurements of spontaneous oscillations for moderate-size raindrops. *J. Atmos. Sci.*, **50,** 1089–1098.

Maguire, W. B., and S. K. Avery, 1994: Retrieval of raindrop size distributions using two Doppler wind profilers: Model sensitivity testing. *J. Appl. Meteor.*, **33,** 1623–1635.

Matrosov, S. Y., R. A. Kropfli, R. F. Reinking, and B. E. Martner, 1999: Prospects for measuring rainfall using propagation differential phase in X- and K_a-radar bands. *J. Appl. Meteor.*, **38,** 766–776.

May, P. T., A. R. Jameson, T. Keenan, P. Johnson, and W. Ecklund, 1999a: Combined wind profiler/polarimetric radar studies of the vertical motion and microphysical characteristics of sea breeze thunderstorms. Preprints, *29th Int. Conf. on Radar Meteorology*, Montreal, PQ, Canada, Amer. Meteor. Soc., 247–350.

——, T. D. Keenan, D. S. Zrnić, L. D. Carey, and S. A. Rutledge, 1999b: Polarimetric measurements of rain at a 5-cm wavelength. *J. Appl. Meteor.*, **38,** 750–765.

Mueller, E. A., 1984: Calculation procedures for differential propagation phase shift. Preprints, *22d Conf. on Radar Meteorology*, Zurich, Switzerland, Amer. Meteor. Soc., 397–399.

Pruppacher, H. R., and K. V. Beard, 1970: A wind tunnel investigation of the internal circulation and shape of water drops falling at terminal velocity in air. *Quart. J. Roy. Meteor. Soc.*, **96,** 247–256.

Rajopadhyaya, D. K., P. T. May, and R. A. Vincent, 1993: A general approach to the retrieval of rain-drop-size distributions from VHF wind profiler Doppler spectra: Modeling results. *J. Atmos. Oceanic Technol.*, **10,** 710–717.

——, ——, R. Cifelli, S. K. Avery, C. Williams, W. L. Ecklund, and K. S. Gage, 1998: The effect of vertical air motions on rain rates and median volume diameter determined from combined UHF and VHF wind profiler measurements and comparisons with rain gauge measurements. *J. Atmos. Oceanic Technol.*, **15,** 1306–1319.

——, S. K. Avery, P. T. May, and R. C. Cifelli, 1999: Comparison of precipitation estimation using single- and dual-frequency wind profilers: Simulations and experimental results. *J. Atmos. Oceanic Technol.*, **16,** 165–173.

Rasmussen, R. M., V. Levizzani, and H. R. Prupacher, 1984: A wind tunnel and theoretical study on the melting behavior of atmospheric ice particles: III. Experiment and theory for spherical ice particles of radius >500 μm. *J. Atmos. Sci.*, **41,** 381–388.

Rogers, R. R., 1967: Doppler radar investigations of Hawaiian rain. *Tellus*, **19,** 432–455.

——, D. Baumgardner, S. A. Ether, D. A. Carter, and W. L. Ecklund, 1993: Comparison of raindrop size distributions measured by radar wind profiler and by airplane. *J. Appl. Meteor.*, **32,** 694–699.

Sachidananda, M., and D. S. Zrnić, 1986: Differential propagation phase shift and rainfall rate estimation. *Radio Sci.*, **21,** 235–247.

Sato, T., H. Doji, H. Iwai, and I. Kimura, 1990: Computer processing for deriving drop-size distributions and vertical air velocities from VHF Doppler radar spectra. *Radio Sci.*, **25,** 961–973.

Sekhon, R. S., and R. C. Srivastava, 1971: Doppler radar observations of drop-size distributions in a thunderstorm. *J. Atmos. Sci.*, **28,** 983–994.

Seliga, T. A., and V. N. Bringi, 1976: Potential use of a radar differential reflectivity measurements at orthogonal polarizations for measuring precipitation. *J. Appl. Meteor.*, **15,** 69–76.

Vivekanandan, J., V. N. Bringi, and R. Raghavan, 1990: Multiparameter radar modeling and observations of melting ice. *J. Atmos. Sci.*, **47,** 549–564.

Wakasugi, K., A. Mizutani, M. Matsuo, S. Fukao, and S. Kato, 1986: A direct method for deriving drop-size distribution and vertical air velocities from VHF Doppler radar spectra. *J. Atmos. Oceanic Technol.*, **3,** 623–629.

Zahrai, A., and D. S. Zrnić, 1993: The 10 cm-wavelength polarimetric weather radar at NOAA's National Severe Storms Laboratory. *J. Atmos. Oceanic Technol.*, **10,** 649–662.

Zrnić, D. S., and A. Ryzhkov, 1996: Advantages of rain measurements using specific differential phase. *J. Atmos. Oceanic Technol.*, **13,** 454–464.

——, and ——, 1999: Polarimetry for weather surveillance radars. *Bull. Amer. Meteor. Soc.*, **80,** 389–406.